THE JOURNAL OF BIOLOGICAL CHEMISTRY VOL. 286, NO. 17, pp. 14913–14921, April 29, 2011

Arabidopsis Membrane-anchored Ubiquitin-fold (MUB) Proteins Localize a Specific Subset of Ubiquitin-conjugating (E2) Enzymes to the Plasma Membrane*[S]

Received for publication, June 25, 2010, and in revised form, February 21, 2011 Published, JBC Papers in Press, February 23, 2011, DOI 10.1074/jbc.M110.158808

Rebecca T. Dowil[‡], Xiaolong Lu[‡], Scott A. Saracco[§], Richard D. Vierstra[¶1], and Brian P. Downes[‡2]

From the [‡]Department of Biology, Saint Louis University, St. Louis, Missouri 63103-2010, the [¶]Department of Genetics, University of Wisconsin, Madison, Wisconsin 53706-1574, and [§]Monsanto Company, St. Louis, Missouri 63017

The covalent attachment of ubiquitin (Ub) to various intracellular proteins plays important roles in altering the function, localization, processing, and degradation of the modified target. A minimal ubiquitylation pathway uses a three-enzyme cascade (E1, E2, and E3) to activate Ub and select target proteins for modification. Although diverse E3 families provide much of the target specificity, several factors have emerged recently that coordinate the subcellular localization of the ubiquitylation machinery. Here, we show that the family of membrane-anchored ubiquitin-fold (MUB) proteins recruits and docks specific E2s to the plasma membrane. Protein interaction screens with *Arabidopsis* MUBs revealed that interacting E2s are limited to a well defined subgroup that is phylogenetically related to human UbcH5 and yeast Ubc4/5 families. MUBs appear to interact noncovalently with an E2 surface opposite the active site that forms a covalent linkage with Ub. Bimolecular fluorescence complementation demonstrated that MUBs bind simultaneously to the plasma membrane via a prenyl tail and to the E2 *in planta*. These findings suggest that MUBs contribute subcellular specificity to ubiquitylation by docking the conjugation machinery to the plasma membrane.

Protein ubiquitylation is a reversible post-translational modification regulating target protein activity, localization, and degradation in diverse signaling pathways (1, 2). The fate of a ubiquitin (Ub)[3]-targeted protein ultimately depends on the length and linkage of the attached Ub molecules (3). For instance, Ub Lys[48]-linked chains typically direct target proteins into the Ub/26 S proteasome system (UPS) for degradation. Ubiquitylation at the plasma membrane often differs from the canonical UPS through reversible monoubiquitylation, protein recycling between the membrane and endomembrane systems, the assembly of Lys[63]-linked chains, and terminal lysosomal targeting (4). For example, monoubiquitylation of plasma membrane proteins triggers their endocytosis (1, 3, 5, 6).

Ub and related proteins are part of the β-grasp protein structure family that is characterized by a transverse α-helix cradled in a five-stranded β-sheet. The C-terminal diglycine of Ub is necessary for activation by an E1 enzyme, transfer to the active site of a Ub-conjugating enzyme (UBC; E2), and covalent attachment to a target protein guided by an E3 enzyme. Ub-related proteins should be considered either Ub-like when they are used in a covalent protein conjugation reaction or, if not, simply Ub-fold. Functional variation in protein conjugation is attributed to a growing list of Ub-like proteins, including SUMO (small ubiquitin-like modifier), RUB (NEDD8), UFM, and others (7). Alternatively, Ub-fold proteins, which lack a C terminus for protein conjugation, use the β-grasp for protein interactions that guide subcellular organization of ubiquitylation. For instance, RAD23 directs ubiquitylated cargoes to the 26 S proteasome, and phosphatidylethanolamine-conjugated ATG8 marks membranes in developing autophagosomes (8, 9).

Throughout the UPS, the Ub-fold is recognized by various Ub-binding domains (UBDs) from the initial E1 enzyme (10) to the Ub conjugate docking 26 S proteasome subunits RPN1, RPN10, and RPN13 (11). An Ile[44]-centered hydrophobic surface on the exterior of the Ub β-sheet is most commonly recognized by UBDs. Certain E2s can also interact with this surface without encroaching on their active site. Specifically, solution-based two-dimensional NMR studies detected Ub bound noncovalently near Ser[22] on human (*Homo sapiens* (Hs)) UbcH5c (12), which has been confirmed by activity assays (13, 14) and crystallography (14) for HsUbcH5b. Noncovalent Ub-E2 interaction is proposed to aid assembly of Ub-E2 polymeric complexes for enhanced target protein polyubiquitylation (12, 14). Ub enzyme variants (UEVs) resemble E2s but lack an active site cysteine, thus precluding covalent conjugation to Ub-like proteins. Nevertheless, UEVs can diversify E2 activities (15–17). In fact, a noncovalent interaction between Ub and the UEV Mms2 promotes the UEV/E2 heterodimer Mms2/Ubc13 to form Lys[63]-linked poly-Ub chains (16). In yeast, a related noncovalent interaction between SUMO and its E2, Ubc9, also stimulates poly-SUMO chain formation (18–23).

Membrane-anchored Ub-fold (MUB) proteins are recent additions to the β-grasp structure family. Compared with Ub,

* This work was supported by Saint Louis University and a Beaumont faculty development grant (to B. P. D.).

This paper is dedicated to the memory of Tim Tague (September 24, 1955 to October 23, 2006), father of Rebecca T. Dowil.

[S] The on-line version of this article (available at http://www.jbc.org) contains supplemental Figs. 1–4 and Tables I and II.

[1] Supported by National Science Foundation *Arabidopsis* 2010 Program Grant MCB-0115870.

[2] To whom correspondence should be addressed: Dept. of Biology, Saint Louis University, 3507 Laclede Ave., St. Louis, MO 63103-2010. Tel.: 314-977-3913; Fax: 314-977-3658; E-mail: bdownes1@slu.edu.

[3] The abbreviations used are: Ub, ubiquitin; UPS, Ub/26 S proteasome system; UBC, Ub-conjugating enzyme; UBD, Ub-binding domain; Hs, *H. sapiens*; UEV, Ub enzyme variant; MUB, membrane-anchored Ub-fold; At, *A. thaliana*; Co-IP, co-immunoprecipitation; BiFC, bimolecular fluorescence complementation; GUS, β-glucuronidase; NLS, nuclear localization signal; Y2H, yeast two-hybrid; SUMO, small ubiquitin-like modifier.

Arabidopsis thaliana (At) MUB1 (Protein Data Bank code 1SE9) and HsMUB (previously known as UBL3; code 2GOW) show strong three-dimensional similarity in the β-grasp, but longer N and C termini and extended loops create MUB-unique surfaces (24–26). MUBs are distinguished from other Ub-fold proteins by a C-terminal C*AAX* box that is modified through protein prenylation with a hydrophobic membrane anchor. Prenylation and membrane localization preclude attachment of MUBs to target proteins. MUBs from nematodes, insects, fish, and mammals, including humans, are prenylated *in vitro* (26). *In planta*, AtMUB membrane localization is prenylation-dependent, where mutation of the prenyl attachment C*AAX* cysteine to a serine (S*AAX*) prevents processing and causes accumulation of non-membrane-localized MUB. Likewise, *Arabidopsis* prenyltransferase mutants block membrane localization of endogenous AtMUB1 (26). The six *MUB* genes of *Arabidopsis* are divided by sequence homology into three subgroups, *MUB1/2*, *MUB3/4*, and *MUB5/6*, suggesting functional diversification of plant MUBs. In contrast, multicellular fungi and animals have only a single *MUB* gene, and no *MUB* gene is evident in yeast (26). Although the structure and post-translational prenyl modifications of MUBs have been well characterized, the function of these Ub-fold proteins is unknown.

In this work, we demonstrate that AtMUB proteins interact with a specific subgroup of E2s. We provide evidence that MUBs directly interact with an E2 noncovalent binding surface *in vitro* and validate the interaction *in planta* by co-immunoprecipitation (Co-IP) and bimolecular fluorescence complementation (BiFC). From these data, we propose that MUB proteins contribute subcellular specificity to the ubiquitylation system by recruiting specific E2s to the plasma membrane.

EXPERIMENTAL PROCEDURES

Phylogenetic Sequence and Structure Analyses—E2 amino acid sequences were trimmed to core domains as identified previously (27). Initial pairwise alignment of the sequences was done in ClustalX2 (28) using the PAM350 protein weight matrix permitting gap opening and extension penalties of 35.0 and 0.75. Final alignment (supplemental Fig. 1) was manually performed with Se-Al Version 2.0a11 (29). The reported phylogenetic tree is the strict consensus of three possible trees generated by a maximum parsimony full heuristic search in PAUP* Version 4.0b10 (30) with AtUFC1 (E2 for UFM1) as an outgroup. Bootstrap support was determined with 1000 pseudoreplicates by the TBR branch swapping algorithm and mapped onto the strict consensus. Alignments were annotated for identity and conservation using Jalview Version 2.5 (31, 32). Protein structures for AtMUB1 (Protein Data Bank code 1SE9) and Ub-UbcH5c (code 2FUH) from the NCBI Molecular Modeling Structure Data Base were annotated using the PyMOL viewer.

Vectors and Plasmid Construction—All Gateway™ entry and ligation cloned vectors were verified by sequencing. Primer sequences for entry vectors and mutagenesis are listed in supplemental Table I. For Gateway™ cloning (Invitrogen), genes within entry vectors were recombined into destination vectors by LR Clonase II reactions and confirmed by restriction mapping. All Gateway cloned constructs are summarized in supplemental Table II. Amino acid substitutions in *AtMUB* and *AtUBC* genes were made following the QuikChange site-directed mutagenesis protocol (Stratagene). *Arabidopsis* E2 genes, excluding *AtUBC7* and *AtUBC23*, were obtained from the *Arabidopsis* Biological Resource Center (Columbus, OH) as cDNA clones in pDONR201 (27) (supplemental Table II). Construction of plasmids pDEST-GBKT7 (33); pACT2.2gtwy (Addgene plasmid 11346); pEarleyGate (pEG) 100, pEG104, pEG201, and pEG202 (34); pGGWA and pHGWA (35); pET28a-UbcH5c and pET28a-UbcH5c S22R (Addgene plasmids 12643 and 12644) (12); and pET28b-*AtMUB1–6* (26) was described previously. The pSAT1-CAMBIA-nEYFP-C1 and pSAT1-CAMBIA-cEYFP-C1 N-terminal split YFP BiFC transformation vectors were constructed with expression cassettes from pSAT1-nEYFP-C1 and pSAT1-cEYFP-C1 (36) inserted into pCAMBIA0380 (37).

To create Gateway entry vectors, *AtMUB3* and *AtMUB4* were PCR-amplified from published pET28 vectors (26) with forward primers including a 5′-CACC sequence and reverse primers designating 3′-C*AAX* or 3′-S*AAX*; products were directionally cloned into pENTR/D-TOPO (Invitrogen). *AtCOP10* and *AtUEV1B* were amplified from *Columbia-0* cDNA and *HsMUB* from SK-HEP cDNA (38) and similarly cloned into pENTR/D-TOPO. The *AtCOP10* splice variant At3g13550.1 was gel-excised prior to D-TOPO cloning. For the FLAG-tagged β-glucuronidase (GUS) control vector, PCR-modified pENTR-GUS (Invitrogen) was recombined into pEG202 (supplemental Table II).

The mCerulean plant nuclear marker was created by PCR amplifying the N-terminal nuclear localization signal (NLS) of *AtZFP11* (At2g42410) (39) from *Columbia-0* genomic DNA with primers adding a 5′-CACC and a 3′-XhoI site and inserted into pENTR/D-TOPO. The mCerulean sequence was PCR-amplified from pmCerulean-C1 (40) to include a C-terminal stop codon (*) and flanking XhoI sites, ligated into similarly cut pENTR/D-TOPO+ZFP11(NLS), sequence-confirmed, and recombined into pEG100 (34) to create the binary vector pEG100+ZFP11(NLS):mCerulean*.

Using conventional cloning methods, *AtMUB1–3* and *AtMUB6* (C*AAX* and S*AAX* forms) and Ub were PCR-amplified with flanking 5′-NdeI and 3′-PstI sites and cloned into the pGBKT7 yeast two-hybrid vector (Clontech). *AtMUB4* and *AtMUB5* were PCR-amplified with 5′-EcoRI and 3′-BamHI sites and cloned into pGBKT7. *AtMUB3*, *AtMUB4*, *AtUBC8*, and *AtUBC9* were PCR-amplified from entry vectors with 5′-XhoI and 3′-XbaI sites and cloned into similarly cut pSAT1-CAMBIA BiFC vectors.

Yeast Two-hybrid Analyses—The yeast two-hybrid cDNA library screen was performed by the Molecular Interaction Facility (Madison, WI) following standard protocols (41). Haploid yeast mating strains PJ694A (for *MUB* genes) and PJ694α (for *UBC* and *AtUEV* genes) (42) were transformed using the Frozen-EZ Yeast Transformation II method (Zymo Research Corp.). Yeast cells were grown at 30 °C on complete yeast extract peptone dextrose (YEPD) or synthetic dropout medium lacking amino acids as appropriate for mating and plasmid selection. Sterile 3-amino-1,2,4-triazole at 0.5, 1, 2, or 4 mM

added stringency on synthetic dropout medium lacking histidine. Interaction data are reported only in the absence of growth of empty vector controls. Results were confirmed with standard β-gal filter lift assays (data not shown).

Protein Purification and in Vitro Interaction Studies—Coexpression of AtMUB3 S*AAX* and AtUBC8 was carried out in *Escherichia coli* BL21. All other proteins were expressed in *E. coli* Rosetta 2 (Novagen). Expression of His_6-tagged AtMUB3 was induced with 0.2 mM isopropyl 1-thio-β-D-galactopyranoside for 12 h at 19 °C. Cells were extracted by ultrasonication in PBS (20 mM phosphate and 200 mM NaCl, pH 6.8) and clarified by centrifugation. PMSF was maintained at 1 mM throughout purification. Extract was incubated with TALON metal affinity resin (Clontech) for 30 min, followed by three washes with 10 mM imidazole/PBS, three washes with 50 mM imidazole/PBS, and elution with 250 mM imidazole/PBS. Expression of GST-tagged AtUBC8 and AtUBC8(S22R) was induced as described above, and soluble protein extracts were incubated with immobilized GSH resin (Thermo Scientific) for 30 min, followed by three washes with PBS. GST-tagged proteins were eluted in 15 mM reduced GSH/PBS. For pulldown assays, GST-tagged AtUBC8 or AtUBC8(S22R) was immobilized on GSH resin, mixed with purified His_6-tagged AtMUB3 for 30 min, washed three times with PBS, and boiled in Laemmli sample buffer. All purifications were analyzed by SDS-PAGE and Coomassie Blue staining or immunoblotting as appropriate.

Agrobacterium Infiltration, Co-IP, and BiFC—Binary vectors were transformed into *Agrobacterium tumefaciens* strain GV3101 by electroporation. Cells from an overnight culture were washed with sterile 20 mM $MgSO_4$ and suspended in an equal volume of infiltration buffer (10 mM MES, 10 mM $MgSO_4$, and 100 μM acetosyringone, pH 5.2). Bacterial infiltration solutions were incubated for 3 h at 25 °C with shaking before mixing the cultures as appropriate and infiltrating into young, nearly expanded *Nicotiana benthamiana* leaves. Plants (3–5 weeks old) grown in 16 h long days under fluorescent light were kept in the dark for 2 days following infiltration before being returned to the light for 1 day. Cells were imaged by confocal microscopy with a Zeiss LSM 5 microscope using an argon laser. The YFP signal was obtained with 514 nm excitation with HFT 458/514, NFT 545, and BP 530–600 filters. For negative controls, cells within infiltrated regions of tissue were imaged. Autofluorescence was excited at 514 nm and collected with HFT 458/514, NFT 545, and LP 650 filters, and mCerulean was excited at 458 nm and collected with HFT 458/514/633, NFT 490, and BP 475–525 filters. Image brightness and contrast adjustments and overlays were done with NIH ImageJ Version 1.44b.

For Co-IP studies, *Agrobacterium* cultures were normalized to $A_{600} = 0.6$ in infiltration buffer, mixed, and co-infiltrated. *N. benthamiana* tissue was ground with 3 volumes (w/v) of prechilled extraction buffer (50 mM Tris adjusted to pH 8.0 with MES, 0.5 M sucrose, 1 mM $MgCl_2$, 10 mM EDTA, and 5 mM DTT) adapted from Liu *et al.* (43) with 1 mM PMSF and 1:100 plant protease inhibitor mixture (Sigma) in a 4 °C cold room. The homogenate was centrifuged at 4000 × *g* for 15 min and clarified again at 2000 × *g* for 10 min. Total protein was quantified by Coomassie Plus assay (Pierce), and samples were normalized to 2 mg/ml. The supernatant was incubated with anti-FLAG M2 affinity gel (Sigma) for 1 h at 4 °C, washed three times with PBS with 0.05% Tween 20, boiled with Laemmli sample buffer, and analyzed by SDS-PAGE and immunoblotting with anti-HA-HRP and anti-FLAG antibodies (Sigma).

RESULTS

Yeast Two-hybrid Screen Reveals MUB-interacting E2s—AtMUB1 was used as bait in a Gal4 yeast two-hybrid (Y2H) *Arabidopsis* cDNA screen of >18 million clones representing mRNA from tissues, cultured cells, and diverse physiological conditions (Molecular Interaction Facility) and identified multiple occurrences of three E2s, AtUBC8–10, with 20, 2, and 5 hits, respectively. To facilitate nuclear interaction of the Gal4 transcriptional subunits, a prenylation-deficient mutant, AtMUB1 S*AAX* (which corresponds to C114S), was used as bait. In directed Y2H experiments, both WT C*AAX* and prenylation-deficient S*AAX* forms of AtMUBs interacted with AtUBC8–10, but results using the S*AAX* versions were most consistent (data not shown). Therefore, *MUB* S*AAX* bait constructs were used in subsequent experiments.

Arabidopsis MUBs Specifically Interact with Subgroup VI E2s—Directed Y2H experiments were performed to determine whether MUBs interact with additional E2s that were undetected due to gene expression bias in the cDNA library and to establish an interaction pattern between MUBs and E2s. Thirty-seven AtUBCs were organized into 14 subgroups by Kraft *et al.* (27) based on the phylogenetic relationship of the enzymatic core domain. This diverse *Arabidopsis* E2 family is represented in Fig. 1*A* with additional gene structure characteristics that validate the well supported sequence relationships (bootstrap support in Fig. 1*A*). Haploid yeast strains for all six AtMUB S*AAX* and Ub baits were crossed with all 14 E2 subgroups as prey. In total, 35 of 37 *Arabidopsis* E2s and two UEVs, AtCOP10 and AtUEV1B (MMZ2), were examined. AtUEV1B was tested because it is an *Arabidopsis* homolog of Mms2 (17), and it contains a C-terminal C*AAX* (CCVM) signal that might localize it with MUBs at a membrane. AtCOP10 was tested because, among the UEV family members, it is most closely related to AtUBC8–10 (Fig. 1*A*). In this comprehensive directed survey of MUB-E2 interactions, all six AtMUBs interacted with E2s, confirming the AtMUB1 library screen results (Fig. 1*B*).

AtMUBs interacted exclusively with Subgroup VI E2s, including AtUBC8–10, as detected in the initial Y2H screen, and also with AtUBC11 and AtUBC28–30 (Fig. 1*B*). AtUBC12 and AtUBC19 failed to interact but were excluded from further analysis because growth was auto-activated with various empty bait vector controls. Within the positive Subgroup VI interactions, MUBs showed a combinatorial pattern of interaction with E2s. For instance, AtUBC9 interacted with all six AtMUBs, whereas AtUBC11 and AtUBC30 interacted only with the AtMUB3/4 subgroup (Fig. 1*B*). Ironically, the original bait, AtMUB1, showed the weakest E2 interaction profile, only positive for AtUBC8 and AtUBC9 under the assay conditions shown in Fig. 1*B*. No interaction was detected between AtMUBs and a SUMO E2, AtSCE1 (data not shown); between

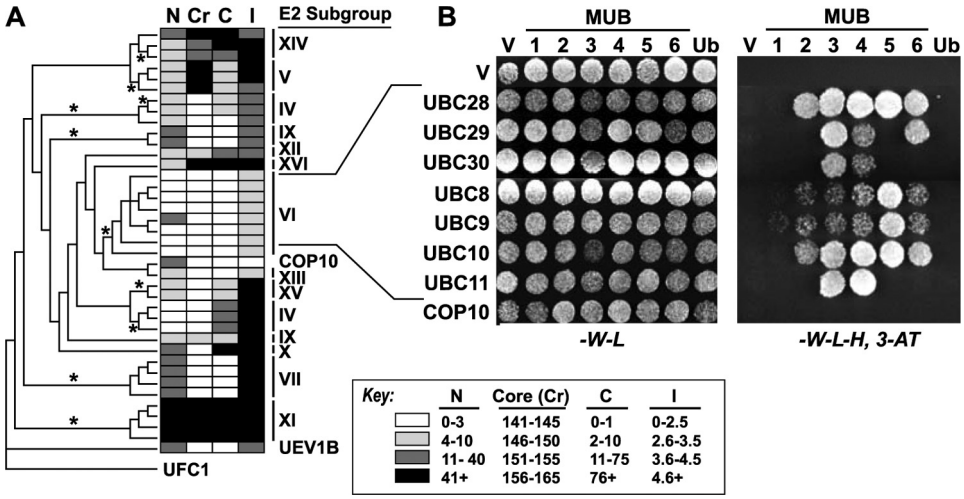

FIGURE 1. ***Arabidopsis* MUBs specifically interact with Subgroup VI E2s.** *A*, a strict consensus phylogenetic tree summarizes the sequence relationship within the core domain of *Arabidopsis* E2s. Subgroups are indicated with *Roman numerals*, as described (23). The tree is rooted to outgroup AtUFC1, the E2 for UFM conjugation. *Asterisks* indicate branches with 100% bootstrap support from 1000 pseudoreplicates. Additional E2 gene characters, including the length of the N-terminal extension (*N*), core domain (*Cr*), and C-terminal extension (*C*) and the average number of introns (*I*), are shaded according to the key (*inset*). *B*, a directed Y2H assay of positive interactions identified in a screen between the baits AtMUB1–6 and Ub and preys AtUBC1–6, AtUBC8–22, AtUBC24–37, AtCOP10, and AtUEV1B. The entire screen and full-size tree are available in supplemental Fig. 2. DNA-binding domain bait constructs and corresponding vector controls (*V*) are on the *horizontal axis*, whereas activation domain prey constructs and vector controls are on the *vertical axis*. Y2H selection is summarized for each panel (*lower*), where amino acid dropouts (−) are indicated: *L*, leucine; *W*, tryptophan; *H*, histidine; *3-AT*, 2 mM 3-amino-1,2,4-triazole.

AtMUBs and AtUEVs; or between Ub and any of the Subgroup VI E2s by Y2H survey.

AtMUB3 and AtMUB4 yeast colonies showed robust growth with the broadest number of E2s and were used for subsequent experiments. AtMUB3 and AtMUB4 are representative of the two prenylation modifications: geranylgeranylation and farnesylation, respectively (26). The AtMUB3/4 subgroup also represents the residue variation seen in the Ub Ile^{44}-homologous surface, where a number of UBDs are known to interact (Fig. 2, *C* and *D*) (24). Mutation of the yeast nonessential T66 residue in Ub to E disrupts binding of UBDs to the Ile^{44} surface while preserving Ub conjugation activity (12, 44). Thr^{66} in Ub is substituted with Val in AtRUB and all known animal and fungal MUBs (26). In *Arabidopsis*, Val and Thr are alternately found at the same position in MUB3 and MUB4, respectively (Fig. 2*C*).

Subgroup VI E2s and MUBs Contain Structure-predicted Noncovalent Interaction Sites—We constructed an alignment of MUB-interacting and MUB-non-interacting E2s to identify any common sequence motif responsible for the Y2H interaction pattern. Fig. 2*A* illustrates sequence identity in a subregion of the E2 core encompassing β-sheets 1–3. As expected, there is high sequence conservation throughout the core, even when comparing representative E2s of distantly related subgroups (supplemental Fig. 1). This relationship is evident in the number of residues with 80% identity, highlighted in *black* in the alignment (Fig. 2*A*). However, the weak overall E2 conservation spanning β-sheets 1 and 2 contrasts with the strong conservation within MUB-interacting E2s including an absolutely conserved Ser^{22}, indicated in Fig. 2*A*.

The MUB-interacting Subgroup VI E2s are closely related to the human UbcH5a–c and yeast Ubc4/5 E2 families. Noncovalent Ub contact residues identified on HsUbcH5b and HsUbcH5c span β-sheets 1–3 and are also conserved in MUB-interacting E2s (Fig. 2, *A* and *B*). We found that HsMUB also interacted with HsUbcH5c by Y2H assay (Fig. 2*E*). In fact, HsMUB interacted with AtUBC8 and AtUBC9, and AtMUB3 and AtMUB4 interacted with HsUbcH5c, demonstrating an evolutionarily conserved interface.

Conserved sequence between *Arabidopsis* MUBs and Ub is depicted in Fig. 2*C*. Ub-E2 contact residues conserved in MUBs form a discrete Ub Ile^{44}-proximal surface including Thr^{66} (Fig. 2*D*) and, in conjunction with E2 conservation, led to the hypothesis that a similar noncovalent interaction occurs between MUBs and Subgroup VI E2s.

MUBs Interact Noncovalently with E2s on a Surface Distinct from the E2 Active Site—To determine whether MUBs and E2s interact in a fashion analogous to Ub and HsUbcH5b/c, mutagenesis was performed in the predicted interaction sites based on the mutations HsUbcH5c (S22R) and Ub (T66E) (12). Homologous V86E and T86E mutations were made in AtMUB3 and AtMUB4, respectively. Likewise, AtUBC8 (S22R) and AtUBC9 (S52R) noncovalent interaction site mutations and active site C85S and C115S mutations were constructed. As shown in Fig. 3, the S22R and S52R mutations in AtUBC8 and AtUBC9 completely abolished MUB-E2 interaction by Y2H assay. The homologous HsUbcH5c (S22R) mutation also interrupted the interaction with HsMUB (supplemental Fig. 3). Similarly, the noncovalent interaction mutants AtMUB3 (V86E) and AtMUB4 (T86E) were unable to interact with either WT or mutant E2s. Alternatively, E2 active site mutations did not interfere with MUB interaction by Y2H assay. Taken together with the strong sequence and structural conservation, these data support the conclusion that MUBs and Ub interact with this versatile E2 interface.

MUBs and E2s Bind Directly in Vitro—To establish whether MUB-E2 binding is dependent upon additional eukaryotic proteins, the interaction was reconstituted *in vitro*. Recombinant purified AtMUB3 was pulled down by GST-AtUBC8 but not by GST-UBC8 (S22R) or GST alone (Fig. 4*A*), demonstrating that

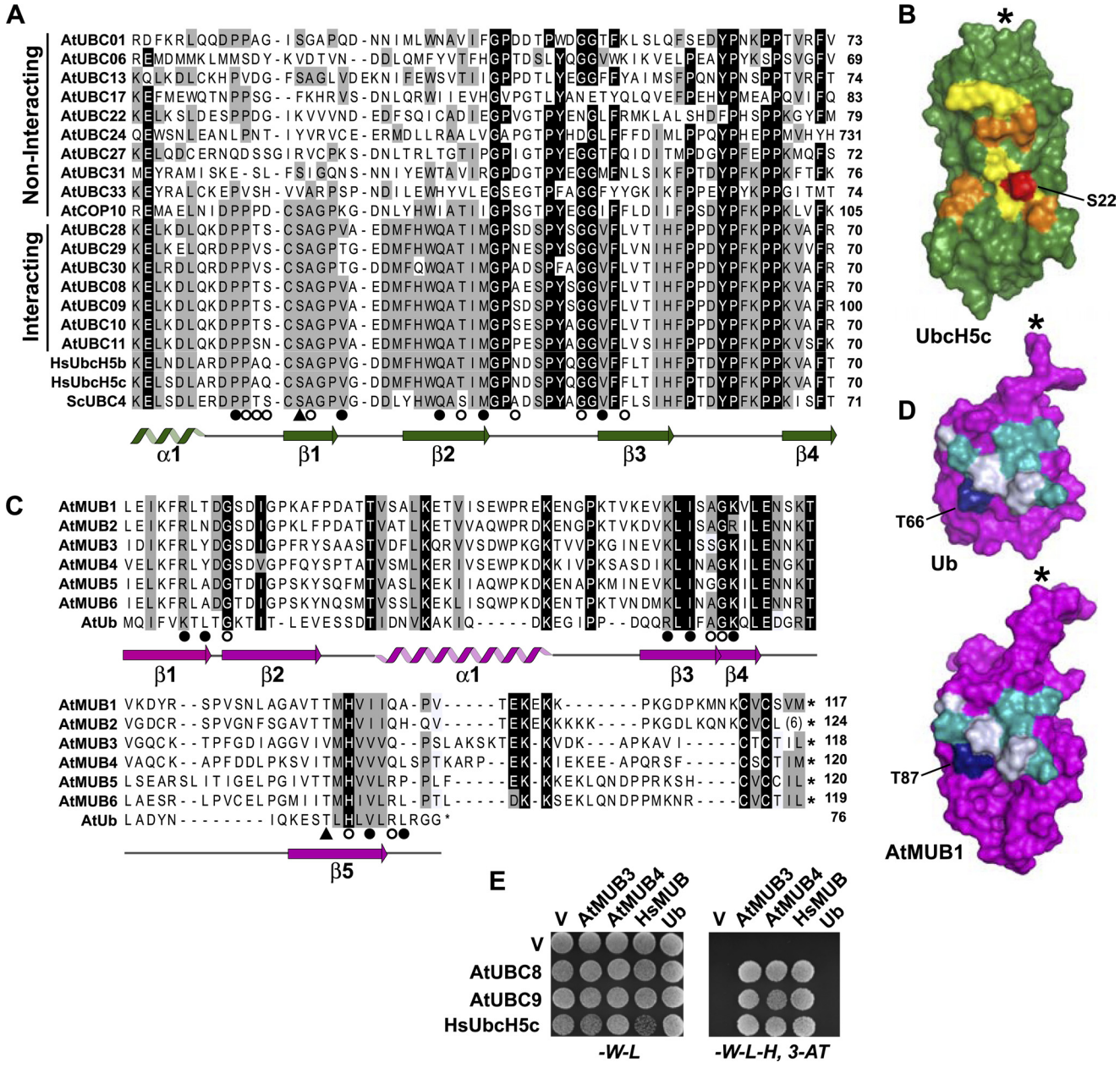

FIGURE 2. ***Arabidopsis* Subgroup VI E2s and MUBs contain structure-predicted noncovalent interaction sites.** *A*, protein sequence alignment of α-helix 1 through β-sheet 4 of MUB-interacting and representative non-MUB-interacting E2s (identified in Fig. 1) is indicated on the *vertical axis*. Sequence identities of 80% (*black*) and 50% (*gray*) are highlighted. Also included are human E2s previously determined to bind Ub in this region, including HsUbcH5c (12) and HsUbcH5b (14). Residues NMR-shifted by Ub noncovalent binding with the HsUbcH5 family are indicated: *closed circles* and *triangles*, HsUbcH5b *and* HsUbcH5c; *open circles*, UbcH5b *or* UbcH5c. The interaction-critical HsUbcH5 Ser^{22} is indicated by a *triangle*. The homologous yeast *Saccharomyces cerevisiae* (*Sc*) Ubc4 is included for reference. *B*, a surface-rendered HsUbcH5c structure (Protein Data Bank code 2FUH) shows the noncovalent Ub-binding interface with the C terminus indicated (*asterisk*). Residues indicated with *circles* or a *triangle* in *A* were colored onto the structure if conserved in MUB-interacting E2s: *orange*, *closed circles* (HsUbcH5 Pro^{16}, Val^{26}, Gln^{34}, Met^{38}, and Val^{49}); *yellow*, *open circles* (HsUbcH5 Pro^{17}, Ala^{23}, Thr^{36}, and Gly^{47}); *red*, *triangle* (HsUbcH5 Ser^{22}). *C*, protein sequence alignment of AtMUBs and Ub. A sequence identity of 80% (*black*) and a conservation index of 50% (*gray*) are highlighted. *D*, residues indicated in *C* with *circles* or a *triangle* were colored onto the structures if conserved between AtMUBs and Ub: *teal*, *closed circles* (Ub Lys^{6}, Arg^{42}, Ile^{44}, Lys^{48}, Thr^{66}, and Val^{70}); *white*, *open circles* (Ub Gly^{10}, Ala^{46}, Gly^{47}, and His^{68}); *blue*, *triangle* (Ub Thr^{66}, AtMUB1 Thr^{87}, AtMUB3 Val^{86}, AtMUB4 Thr^{86}). *E*, a directed Y2H assay demonstrating the interaction of HsUbcH5c with HsMUB, as well as the cross-kingdom interactions of AtMUBs with HsUbcH5c and of HsMUB with AtUBCs. Assay conditions were as described in the legend to Fig. 1, except that 1 mM 3-amino-1,2,4-triazole (*3-AT*) was used. *V*, vector control.

Ser^{22} is required for direct binding to AtMUB3. We were unable to perform the reciprocal experiment because purified AtMUB3 was unstable when reapplied to metal affinity resin. We circumvented this detail by using lysates from *E. coli* coexpressing the proteins. Here, AtUBC8 pulled down AtMUB3 and vice versa, but AtUBC8 (S22R) only weakly bound AtMUB3 (Fig. 4*B*). These *in vitro* assays confirm the Y2H interaction data and also establish that MUB-E2 binding can occur in the absence of additional eukaryotic proteins.

MUB and E2 Noncovalent Interaction Mutations Prevent Co-IP in Planta—To examine the MUB-E2 interface *in planta*, anti-FLAG Co-IP was performed on *N. benthamiana* leaf tissue co-infiltrated with combinations of WT or mutant FLAG-AtMUB3 *CAAX* and HA-AtUBC8 constructs using FLAG-GUS

as a negative control. To compensate for lower AtUBC8 (S22R) expression, three times more total extract was loaded (Fig. 5*A*, *fourth* and *fifth lanes*) and applied to resin relative to WT AtUBC8. WT AtUBC8 coprecipitated only with WT AtMUB3 but not with AtMUB3 (V86E) or GUS. AtUBC8 (S22R) failed to coprecipitate with either WT or mutant AtMUB3 (Fig. 5*A*).

MUBs Localize E2s to the Plasma Membrane in Planta—We additionally sought to identify the localization of the MUB-E2 interaction through BiFC of split YFP. A full-length YFP fusion of AtMUB3 C*AAX* localized to the plasma membrane in *N. benthamiana* leaf cells (Fig. 5*B*). Alternately, YFP-tagged AtMUB3 S*AAX*, AtUBC8, and AtUBC9 all localized in nuclei and the cytoplasm. These MUB localization results in *N. benthamiana* are similar to previous observations in *Arabidopsis* protoplasts and stably transformed plants (26).

When N-terminal YFP-AtMUB3 S*AAX* was co-infiltrated with C-terminal YFP-AtUBC8 or C-terminal YFP-AtUBC9, fluorescence was observed in nuclei and cytoplasmic strands, indicating that the proteins do indeed interact (Fig. 5*C*). Importantly, when N-terminal YFP-AtMUB3 C*AAX* was co-infiltrated with C-terminal YFP-AtUBC8, not only was fluorescence observed, but it was localized to the plasma membrane (Fig. 5, *C* and *D*). The same result was seen with AtMUB3 C*AAX* and AtUBC9. Likewise, AtMUB4 C*AAX* co-infiltration with AtUBC8 or AtUBC9 also localized fluorescence to the plasma membrane (supplemental Fig. 4). Split YFP fusions of MUBs or E2s did not fluoresce when coexpressed with the complementing split YFP empty vector (Fig. 5*C*, *left* and *top panels*). The BiFC experiments demonstrated that transgenic MUB fusions are properly recognized by prenylation machinery in plants and, as predicted, localized to the plasma membrane. These experiments also showed that MUBs and E2s interact *in vivo* and that MUB prenylation and membrane localization are sufficient to, at a minimum, recruit E2s to the plasma membrane.

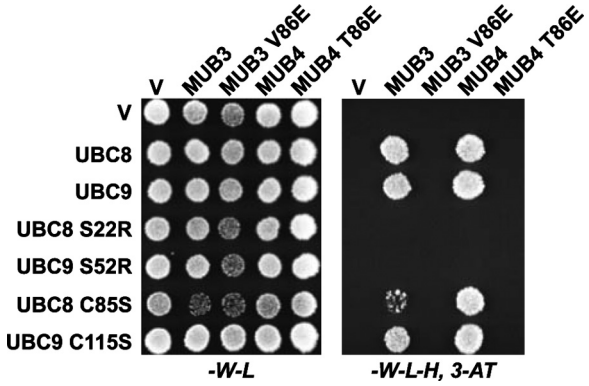

FIGURE 3. ***Arabidopsis* MUBs interact with E2s on a surface distinct from the E2 active site.** Shown are the results from a Y2H mutation analysis of the Ub-HsUbcH5 equivalent noncovalent interaction surfaces of AtMUBs (MUB3 V86E and MUB4 T86E) and AtUBCs (UBC8 S22R and UBC9 S52R) or AtUBC active sites (UBC8 C85S and UBC9 C115S) as described in the legend to Fig. 1, except that 4 mM 3-amino-1,2,4-triazole (*3-AT*) was used. *V*, vector control.

DISCUSSION

Prior to this work, the family of eukaryotic MUB proteins was determined to be associated with the plasma membrane *in vivo* but remained functionally uncharacterized. Here, we have provided the first evidence that MUBs are a direct physical link between the plasma membrane and the ubiquitylation system. Specifically, MUBs recruit a subset of E2s that are defined by a structurally conserved interface, which also interacts noncovalently with Ub (12–14, 45) and possibly other Ub-like proteins.

Y2H, pulldown, and *in planta* Co-IP assays with noncovalent surface mutations identified the interface for the MUB-E2 interaction. Co-IPs performed using MUB C*AAX* proteins paralleled the native localization of MUBs with plasma membrane peripheral proteins. Furthermore, BiFC experiments confirmed the interaction and demonstrated that prenylated MUB proteins can simultaneously bind to the plasma membrane and

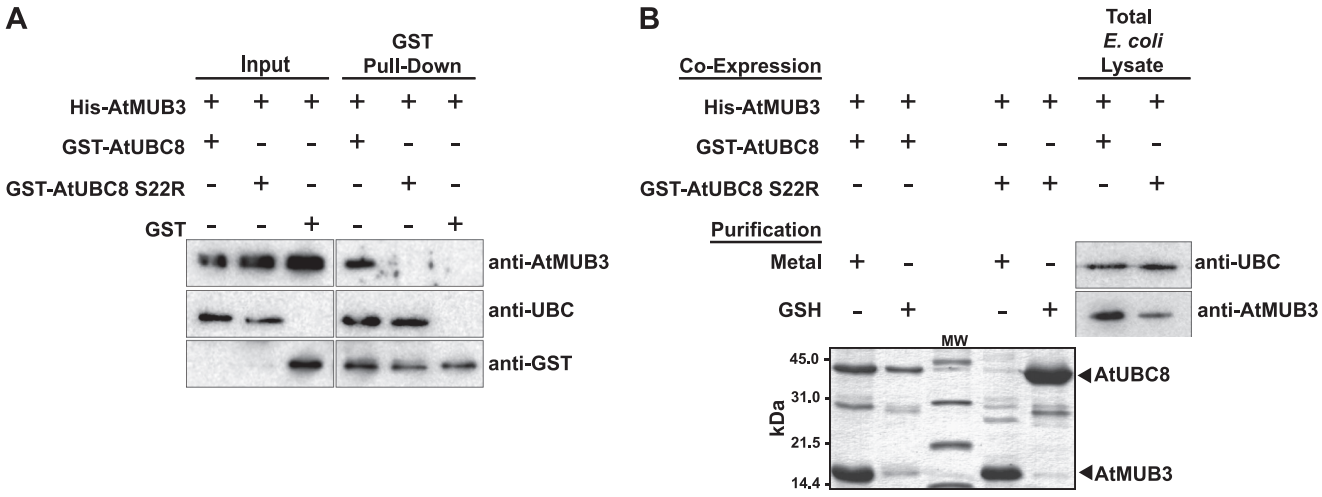

FIGURE 4. ***Arabidopsis* MUBs interact directly with E2s *in vitro*.** *A*, a GST pulldown assay using purified proteins reconstituted MUB-E2 binding *in vitro*. Inputs of recombinant GST-AtUBC8, GST-AtUBC8 S22R, or GST alone were incubated with His-AtMUB3. GSH resin eluates were examined by SDS-PAGE and immunoblotting as indicated. Notably, the interaction was sensitive to the S22R mutation. *B*, *E. coli* coexpression lysates were purified with either GSH resin or TALON His affinity (metal) resin as indicated. Coexpression cultures were achieved with double antibiotic selection for His-AtMUB3 (Amp^r) and GST-AtUBC8 or GST-AtUBC8 S22R (Kan^r). GST-AtUBC8 and His-AtMUB3 proteins copurified efficiently. GST-AtUBC8 S22R and AtMUB3 failed to copurify effectively, as detected by Coomassie Blue, despite similar input protein levels in total *E. coli* lysates detected by immunoblotting as indicated. AtUBC8 and AtMUB3 Coomassie Blue-stained bands are identified with *arrows*. Substoichiometric Coomassie Blue-stained proteins migrating between 21.5 and 31 kDa were recovered with either purification as resin-binding background.

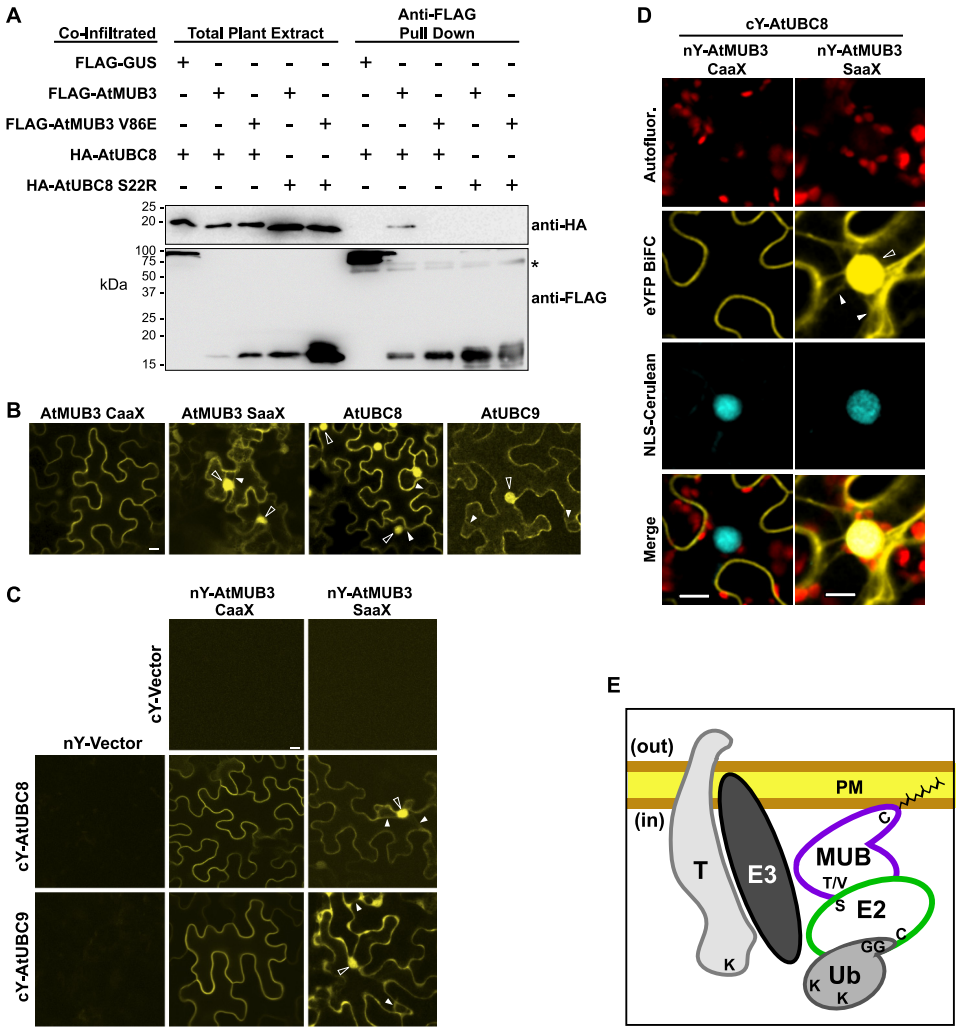

FIGURE 5. ***Arabidopsis* MUBs localize E2s to the plasma membrane *in planta*.** *A*, a Co-IP assay with anti-FLAG resin on *N. benthamiana* leaf tissue cotransformed with WT or mutant combinations of HA-AtUBC8 and FLAG-AtMUB3 *CAAX* or the FLAG-GUS control as indicated. AtUBC8 coprecipitated with AtMUB3 but not with AtMUB3 V86E or GUS. AtUBC8 S22R did not coprecipitate with either AtMUB3 or AtMUB3 V86E. For AtUBC8-containing extracts, 16 μg of total protein was loaded on SDS-polyacrylamide gel representing input, and 450 μg of total protein was applied to 40 μl of anti-FLAG resin. To analyze similar amounts of UBC, three times more AtUBC8 S22R-containing extract was loaded on SDS-polyacrylamide gel and applied to 40 μl of anti-FLAG resin. Equal volumes of FLAG Co-IP eluates were analyzed by SDS-PAGE and immunoblotting as indicated. The *asterisk* indicates mouse IgG cross-reacting bands. *B*, *N. benthamiana* epidermal cells transiently expressing full-length YFP fusions of plasma membrane localized AtMUB3 *CAAX* or cytoplasmic/nuclear localized AtMUB3 *SAAX*, AtUBC8, and AtUBC9. YFP signals localized to cytoplasmic strands (*closed arrowheads*) and nuclei (*open arrowheads*) are indicated. *C*, BiFC of epidermal cells coexpressing split YFP fusions of AtMUB3 and AtUBCs or empty vector controls. Combinations of N- and C-terminal YFP fragments (*nY* and *cY*, respectively) were infiltrated as vector controls or fused to the N terminus of AtMUB and E2 as indicated. AtMUB-E2 interaction and co-localization were observed at the plasma membrane or in the cytoplasm (*closed arrowheads*) and nucleus (*open arrowheads*). *D*, an enlarged view of BiFC with N-terminal YFP-AtMUB3 *CAAX* or N-terminal YFP-AtMUB3 *SAAX* and C-terminal YFP-AtUBC8 highlighting fluorescence in cytoplasmic strands (*closed arrowheads*) and the nucleus (*open arrowhead*). Also shown is chloroplast autofluorescence (*red*) and nuclear localized AtZFP11(NLS)-Cerulean (*blue*). Overlap between YFP and Cerulean is indicated (*white*) in the merged images. *Scale bars* = 10 μm. *E*, a model depicting prenylation-dependent membrane-localized MUB (prenylcysteine (*C*)) tethering an E2 to the inner surface of the plasma membrane (*PM*), leaving the E2 active site (cysteine (*C*)) available to bind the diglycine (*GG*) of Ub. Interaction-critical residues between MUB (*T/V*) and E2 (*S*) are highlighted. Various proteins that could join the complex are indicated in *gray*: Ub, E3, target proteins (*T*), and available lysines (*K*).

to E2s. On the basis of this, we hypothesize that MUBs recruit E2s, perhaps to regulate the homeostasis of active Ub in the plasma membrane-proximal space.

The seven *Arabidopsis* Subgroup VI E2s that interact with MUBs are essentially composed of the core domain, are active with a wide array of E3s (27, 46), and have been characterized extensively *in vitro* (47, 48). Related E2s in animals and fungi, including the human UbcH5 and yeast Ubc4/5 families, have also served as robust model E2s. It is possible that the small size of the Subgroup VI E2s permits access to a diverse array of targets while restricted to the two-dimensional cytoplasmic surface of the plasma membrane. Here, by identifying the capacity to be recruited to the plasma membrane by MUB proteins, we have added a distinguishing biological trait for this E2 family.

We were unable to detect MUB Y2H interactions with E2s outside of this subgroup, including the UEVs AtCOP10 and AtUEV1B (Fig. 1*A* and supplemental Fig. 2). Published NMR studies corroborate that AtCOP10, although sister to the MUB-interacting subgroup, does not interact noncovalently with Ub (13, 15).

The Mms2-related AtUEV1B and the HsUbcH5-related *Arabidopsis* Subgroup VI E2s also did not interact with Ub by Y2H assay. This result is not contradictory because the initial

evaluations of Mms2 and HsUbcH5 with Ub were performed with sensitive NMR-based methods (12, 14, 16). However, this does raise the possibility that MUBs bind Subgroup VI E2s with greater affinity than the Ub-E2 interactions described previously.

Individual subgroup VI E2s likely serve specialized functions *in planta*, as suggested by the combinatorial pattern of Y2H interactions with MUBs. For instance, the AtUBC29 and AtUBC30 proteins are 95% similar with comparable expression *in planta* (27), but only AtUBC29 interacts with AtMUB6. This pattern echoes previously described combinatorial UPS interactions among SCF (for Skp1, Cullin, F-box) E3 subunits (49) or between an E3 and multiple E2s (46). The modular AtMUB and E2 interactions are consistent with an expanded plant UPS compared with animals and fungi (46, 48, 49). Regardless of the species, MUBs may help refine ubiquitylation target selection, reaction dynamics, or localization.

MUB prenylation and E2 binding ability are reminiscent of Pex22p and Cue1p localizing E2s to the endoplasmic reticulum and peroxisome membranes, respectively. In yeast, the transmembrane protein Pex22p recruits the E2 Pex4p to the outer peroxisomal membrane, causing monoubiquitylation and export of Pex5p to the cytoplasm (50, 51). This process appears to be conserved in plants, as a functionally equivalent AtPEX4-AtPEX22 complex is needed to sustain peroxisome biogenesis (52, 53). Also in yeast, the transmembrane protein Cue1p recruits the E2 Ubc7p to the cytoplasmic surface of the endoplasmic reticulum for endoplasmic reticulum-associated degradation of errant proteins (54–57). Now, with the addition of MUBs, a theme emerges in which small adapter proteins anchor E2s to the cytoplasmic surface of specific membranes. Future studies will determine whether MUBs also mediate Ub-directed movement of membrane proteins into the cytoplasm like Pex22p and Cue1p.

In the simplest model, MUBs could recruit an activated E2 to the plasma membrane to donate its Ub to a target or an elongating Ub chain (Fig. 5*E*). Alternatively, the recruited E2 could donate its Ub to Ub-equivalent Lys^{29}, Lys^{48}, or Lys^{63} (26) on a MUB protein. Ubiquitylation of these lysines would present mono-Ub for UBD docking or establish membrane-localized reservoirs of various Ub chains.

MUBs may also influence the dynamics of polyubiquitylating complexes. Recent studies have identified that noncovalent Ub interactions with E2s are important for regulating Ub chain formation (12–14, 19, 45). HsUbcH5c noncovalent interaction with Ub and the subsequent formation of high molecular weight $(Ub\sim E2)_n$ polymers are required for auto-polyubiquitylation of the E3 BRCA1 (12). Here, the S22R mutant of HsUbcH5c is unable to support $(Ub\sim E2)_n$ polymer formation but can still sustain auto-monoubiquitylation of BRCA1 *in vitro* (12–14, 45). The shared use of the E2 noncovalent interaction surface by MUB and Ub poses several possibilities where MUBs influence Ub chain formation (Fig. 5*E*). MUB competition with Ub for noncovalent E2 binding could promote monoubiquitylation of membrane substrates by causing a localized disruption in $(Ub\sim E2)_n$ polymer formation. In contrast, MUBs could take the place of a terminal Ub in a $(Ub\sim E2)_n$ polymer to facilitate the rapid assembly of poly-Ub chains on a membrane target. Furthermore, the binding of MUB to E2s could affect E2 activity regarding chain linkage specificity (58), enzymatic rate (15, 27), and E3 selection (27, 46). Although the impact of MUB-E2 binding at the plasma membrane is uncertain, these models highlight the potential for key advances in understanding ubiquitylation at the plasma membrane and warrant further investigation.

Acknowledgments—Protein expression vectors pGGWA and pHGWA were generous gifts from Didier Busso. pACT2.2gtwy was created by Guy Caldwell. BiFC binary plasmids pSAT1-CAMBIA-nEYFP-C1 and pSAT1-CAMBIA-cEYFP-C1 were gifts from Sona Pandey. The pmCerulean-C1 plasmid template was a gift from Howard Berg with the permission of David Piston. Human SK-HEP cDNA for HsMUB was a gift from Barrie Bode and Richard Finger. We appreciate the phylogenetic help from Mauricio Diazgranados and Jan Barber; the BiFC advice from Naveen Bisht; the preliminary BiFC assistance using Physcomitrella patens from Julie Thole, Pierre-François Perroud, and Ralph Quatrano; and the use of an ImageQuant LAS 3000 imager from John Chrivia.

REFERENCES

1. Vierstra, R. D. (2009) *Nat. Rev. Mol. Cell Biol.* **10,** 385–397
2. Komander, D. (2009) *Biochem. Soc. Trans.* **37,** 937–953
3. Woelk, T., Sigismund, S., Penengo, L., and Polo, S. (2007) *Cell Div.* **2,** 11
4. Hicke, L., Schubert, H. L., and Hill, C. P. (2005) *Nat. Rev. Mol. Cell Biol.* **6,** 610–621
5. Dupré, S., Urban-Grimal, D., and Haguenauer-Tsapis, R. (2004) *Biochim. Biophys. Acta* **1695,** 89–111
6. Hicke, L., and Dunn, R. (2003) *Annu. Rev. Cell Dev. Biol.* **19,** 141–172
7. Downes, B., and Vierstra, R. D. (2005) *Biochem. Soc. Trans.* **33,** 393–399
8. Farmer, L. M., Book, A. J., Lee, K. H., Lin, Y. L., Fu, H., and Vierstra, R. D. (2010) *Plant Cell* **22,** 124–142
9. Geng, J., and Klionsky, D. J. (2008) *EMBO Rep.* **9,** 859–864
10. Lee, I., and Schindelin, H. (2008) *Cell* **134,** 268–278
11. Fu, H., Lin, Y. L., and Fatimababy, A. S. (2010) *Trends Plant Sci.* **15,** 375–386
12. Brzovic, P. S., Lissounov, A., Christensen, D. E., Hoyt, D. W., and Klevit, R. E. (2006) *Mol. Cell* **21,** 873–880
13. Brzovic, P. S., and Klevit, R. E. (2006) *Cell Cycle* **5,** 2867–2873
14. Sakata, E., Satoh, T., Yamamoto, S., Yamaguchi, Y., Yagi-Utsumi, M., Kurimoto, E., Tanaka, K., Wakatsuki, S., and Kato, K. (2010) *Structure* **18,** 138–147
15. Lau, O. S., and Deng, X. W. (2009) *Biochem. J.* **418,** 683–690
16. Lewis, M. J., Saltibus, L. F., Hau, D. D., Xiao, W., and Spyracopoulos, L. (2006) *J. Biomol. NMR* **34,** 89–100
17. Wen, R., Torres-Acosta, J. A., Pastushok, L., Lai, X., Pelzer, L., Wang, H., and Xiao, W. (2008) *Plant Cell* **20,** 213–227
18. Duda, D. M., van Waardenburg, R. C., Borg, L. A., McGarity, S., Nourse, A., Waddell, M. B., Bjornsti, M. A., and Schulman, B. A. (2007) *J. Mol. Biol.* **369,** 619–630
19. Knipscheer, P., van Dijk, W. J., Olsen, J. V., Mann, M., and Sixma, T. K. (2007) *EMBO J.* **26,** 2797–2807
20. Bencsath, K. P., Podgorski, M. S., Pagala, V. R., Slaughter, C. A., and Schulman, B. A. (2002) *J. Biol. Chem.* **277,** 47938–47945
21. Capili, A. D., and Lima, C. D. (2007) *J. Mol. Biol.* **369,** 608–618
22. Liu, Q., Jin, C., Liao, X., Shen, Z., Chen, D. J., and Chen, Y. (1999) *J. Biol. Chem.* **274,** 16979–16987
23. Tatham, M. H., Kim, S., Yu, B., Jaffray, E., Song, J., Zheng, J., Rodriguez, M. S., Hay, R. T., and Chen, Y. (2003) *Biochemistry* **42,** 9959–9969
24. de la Cruz, N. B., Peterson, F. C., Lytle, B. L., and Volkman, B. F. (2007) *Protein Sci.* **16,** 1479–1484
25. Vinarov, D. A., Lytle, B. L., Peterson, F. C., Tyler, E. M., Volkman, B. F., and Markley, J. L. (2004) *Nat. Methods* **1,** 149–153

26. Downes, B. P., Saracco, S. A., Lee, S. S., Crowell, D. N., and Vierstra, R. D. (2006) *J. Biol. Chem.* **281,** 27145–27157
27. Kraft, E., Stone, S. L., Ma, L., Su, N., Gao, Y., Lau, O. S., Deng, X. W., and Callis, J. (2005) *Plant Physiol.* **139,** 1597–1611
28. Larkin, M. A., Blackshields, G., Brown, N. P., Chenna, R., McGettigan, P. A., McWilliam, H., Valentin, F., Wallace, I. M., Wilm, A., Lopez, R., Thompson, J. D., Gibson, T. J., and Higgins, D. G. (2007) *Bioinformatics* **23,** 2947–2948
29. Rambaut, A. (1996–2002) *Sequence Alignment (Se-Al) Program*, Version 2.0a11, University of Oxford, Oxford
30. Swofford, D. L. (2003) *PAUP*, Phylogenetic Analysis Using Parsimony (and Other Methods)*, Version 4.0b10, Sinauer Associates Inc. Publishers, Sunderland, MA
31. Waterhouse, A. M., Procter, J. B., Martin, D. M., Clamp, M., and Barton, G. J. (2009) *Bioinformatics* **25,** 1189–1191
32. Livingstone, C. D., and Barton, G. J. (1993) *Comput. Appl. Biosci.* **9,** 745–756
33. Rossignol, P., Collier, S., Bush, M., Shaw, P., and Doonan, J. H. (2007) *J. Cell Sci.* **120,** 3678–3687
34. Earley, K. W., Haag, J. R., Pontes, O., Opper, K., Juehne, T., Song, K., and Pikaard, C. S. (2006) *Plant J.* **45,** 616–629
35. Busso, D., Delagoutte-Busso, B., and Moras, D. (2005) *Anal. Biochem.* **343,** 313–321
36. Citovsky, V., Lee, L. Y., Vyas, S., Glick, E., Chen, M. H., Vainstein, A., Gafni, Y., Gelvin, S. B., and Tzfira, T. (2006) *J. Mol. Biol.* **362,** 1120–1131
37. Hajdukiewicz, P., Svab, Z., and Maliga, P. (1994) *Plant Mol. Biol.* **25,** 989–994
38. Fuchs, B. C., Finger, R. E., Onan, M. C., and Bode, B. P. (2007) *Am. J. Physiol. Cell Physiol.* **293,** C55–C63
39. Dinkins, R. D., Pflipsen, C., and Collins, G. B. (2003) *Plant Sci.* **165,** 33–41
40. Rizzo, M. A., Springer, G. H., Granada, B., and Piston, D. W. (2004) *Nat. Biotechnol.* **22,** 445–449
41. Fields, S., and Song, O. (1989) *Nature* **340,** 245–246
42. James, P., Halladay, J., and Craig, E. A. (1996) *Genetics* **144,** 1425–1436
43. Liu, L., Zhang, Y., Tang, S., Zhao, Q., Zhang, Z., Zhang, H., Dong, L., Guo, H., and Xie, Q. (2010) *Plant J.* **61,** 893–903
44. Sloper-Mould, K. E., Jemc, J. C., Pickart, C. M., and Hicke, L. (2001) *J. Biol. Chem.* **276,** 30483–30489
45. Christensen, D. E., Brzovic, P. S., and Klevit, R. E. (2007) *Nat. Struct. Mol. Biol.* **14,** 941–948
46. Stone, S. L., Hauksdóttir, H., Troy, A., Herschleb, J., Kraft, E., and Callis, J. (2005) *Plant Physiol.* **137,** 13–30
47. Girod, P. A., and Vierstra, R. D. (1993) *J. Biol. Chem.* **268,** 955–960
48. Smalle, J., and Vierstra, R. D. (2004) *Annu. Rev. Plant Biol.* **55,** 555–590
49. Gagne, J. M., Downes, B. P., Shiu, S. H., Durski, A. M., and Vierstra, R. D. (2002) *Proc. Natl. Acad. Sci. U.S.A.* **99,** 11519–11524
50. Platta, H. W., and Erdmann, R. (2007) *Trends Cell Biol.* **17,** 474–484
51. Kragt, A., Voorn-Brouwer, T., van den Berg, M., and Distel, B. (2005) *J. Biol. Chem.* **280,** 7867–7874
52. Khan, B. R., and Zolman, B. K. (2010) *Plant Physiol.* **154,** 1602–1615
53. Zolman, B. K., Monroe-Augustus, M., Silva, I. D., and Bartel, B. (2005) *Plant Cell* **17,** 3422–3435
54. Kostova, Z., Mariano, J., Scholz, S., Koenig, C., and Weissman, A. M. (2009) *J. Cell Sci.* **122,** 1374–1381
55. Biederer, T., Volkwein, C., and Sommer, T. (1997) *Science* **278,** 1806–1809
56. Ravid, T., and Hochstrasser, M. (2007) *Nat. Cell Biol.* **9,** 422–427
57. Koller, A., Snyder, W. B., Faber, K. N., Wenzel, T. J., Rangell, L., Keller, G. A., and Subramani, S. (1999) *J. Cell Biol.* **146,** 99–112
58. David, Y., Ziv, T., Admon, A., and Navon, A. (2010) *J. Biol. Chem.* **285,** 8595–8604